

DATA REPOSITORY 1

To Sink, Swim, Twin, or Nucleate: A critical appraisal of crystal aggregation processes

Penny E. Wieser^{1*}, Zoja Vukmanovic¹, Rüdiger Kilian², Emilie Ringe^{1,3}, Marian B. Holness¹, John Maclennan¹, Marie Edmonds¹

¹ Department of Earth Sciences, University of Cambridge, CB2 3EQ, UK.

² Institute for Geosciences and Geography, University Halle, Germany.

³Department of Materials Science and Metallurgy, University of Cambridge, CB3 0FS, UK.

* Corresponding author: pew26@cam.ac.uk

SAMPLE LOCATIONS

The UG2 chromitite sample was kindly provided by Ilya Veksler. This was collected from the Rustenburg layered suite at Khuseleka mine (25°37'26.73"S, 27°15'22.11"E; see Veksler et al. 2018 for more details).

Olivine dendrites within West Greenland picritic samples were kindly provided by Lotte Larsen (see Larsen and Pederson, 2000 for more details).

Olivine aggregates were analysed from a variety of subaerial eruptions at Kīlauea volcano (see below). The samples are from Kīlauea's East Rift Zone (ERZ), the northern and southern strand of the South West Rift Zone (NSWRZ; SSWRZ), and around the summit caldera (intracaldera if within the summit depression, extracaldera if around the bordering faults).

<u>Sample</u>	<u>Number of aggregates examined</u>	<u>Eruption Date</u>	<u>Location</u>	<u>GPS co-ordinates</u>
KL0909	4	May 24th, 1969	ERZ	19° 21.826' N, 155° 12.877' W
KL0908	29	Dec 30 th , 1969	ERZ	19° 20.839' N, 155° 12.518' W
KL0910	13	Nov 10 th , 1973	ERZ	19° 22.313' N, 155° 13.510' W
KL0916	1	Aug 14 th , 1971	Intracaldera	19° 24.137' N, 155° 16.644' W
KL0917	2	Late July, 1974	Intracaldera	19° 21.06' N, 155° 16.653' W
KL0919	5	Late Dec, 1974	SSWRZ	19° 22.649' N, 155° 17.609' W
KL0920	5	Late Dec, 1974	SSWRZ	19° 22.603' N, 155° 17.713' W
KL0921	7	~1700 AD	SSWRZ	19° 22.989' N, 155° 17.464' W
KL0924	10	Late July, 1974	Extracaldera	19° 24.142' N, 155° 16.896' W
KL0930	15	1919-1920	NSWRZ	19° 21.230' N, 155° 23.892' W
KL0931	2	Sept 24-29 th , 1971	NSWRZ	19° 20.625' N, 155° 21.659' W

SAMPLE PREPARATION

The vesicular nature of the basaltic scoria samples from Kilauea Volcano was not amenable to thin section making. Additionally, due to the high modal proportion of vesicles, few olivines were found within each thin section. Instead, olivines were picked from sieved, jaw crushed material, and mounted in epoxy stubs. Aggregates were identified from the external morphology of crystals in backscatter electron maps. Samples from the UG2 chromitite layer and West Greenland Picrites were made into thin sections.

Epoxy stubs and thin sections were polished with progressively finer silicon pastes, then with colloidal silica using a VibroMet 2 Buehler Vibratory Polisher. A thin carbon coat was applied before EBSD analysis, and a thicker carbon coat was applied for olivine EPMA analysis.

EBSD-CHROMITE AGGREGATES

EBSD data was collected on a FEI sFEG XL30 SEM with an Oxford Nordlys HKL detector in the Department of Physics, University of Cambridge.

SEM Settings		EBSD Settings	
Aperture	3		
Voltage	20kV	Background (frames)	64
Beam Size	5	Gain	10
Sample Tilt	70°	Hough Resolution	60
Working Distance	20mm	Band Detection (min/max)	6/7
Step size	15µm	Reference	Chromite.cry (Aztec database)

EBSD-OLIVINE AGGREGATES

EBSD data was collected on a FEI Quanta 650FEG SEM equipped with a Bruker e-Flash HR EBSD detector in the Department of Earth Sciences, University of Cambridge. Data collection and indexing was performed with Bruker QUANTAX CrystAlign. Step size was varied depending on the size of the aggregate so that each map took ~15-20 mins to collect.

SEM Settings		EBSD Settings	
Aperture	3	Sample-Detector Distance	~14mm
Voltage	20kV	Background (frames)	2
Beam Size	5.5	Gain	10-30
Sample Tilt	70°	Hough Resolution	60
Working Distance	~17-14mm	Band Detection (min/max)	6/12
Step size	3-15µm	Reference	Forsterite (Fe 0.2 MgO 1.8) AMSDB-ID: 0008912
		EBSP resolution	320x240 pixels

EPMA-OLIVINE AGGREGATES

Olivine transects were performed using a Cameca SX100 EPMA in the Department of Earth Sciences, University of Cambridge. Run conditions of 15kv and 20nA were used, with a beam size of 1µm. Count times, calibration materials, and estimates of precision and accuracy calculated from repeated measurements of a San Carlos Olivine secondary standard are shown below.

Element	Calibration Material	Crystal	Peak Count Time	Precision (%) (Std dev/mean)	Accuracy (%) (measured/standard)
Al	Corundum	LTAP	60s	12.3	97.65
Ca	Diopside	PET, LPET	60s, 60s	6.43	93.55
Si	Diopside	TAP	10s	0.85	99.62
Mg	St. Johns Olivine	TAP	20s	0.75	99.06
Fe	Fayalite	LIF	20s	1.83	99.61

EBSD DATA PROCESSING

Calculating Misorientations

Slightly different methods were used to calculate the misorientation between adjacent grains within olivine and chromite aggregates, reflecting the fact that thousands of chromites were present within a single thin section, whereas olivines aggregates were mounted separately in epoxy, and mapped individually.

For a single EBSD map of an olivine aggregate, grains were calculated using the MTEX calcGrains function with a threshold angle of 0.5° . The positions of the resulting grain boundaries were then compared to BSE images, and only those separating morphologically distinct grains were selected, discarding low angle boundaries in the interior of grains. Then, misorientations were calculated by comparing the mean orientation of adjacent grains selected by the user (Fig. DR1). The traditional approach of calculating misorientations along grain boundaries was not used due to the common presence of residual melt along boundaries. For each map, the resulting misorientation axis and angle were saved as a MATLAB variable. These variables were then combined for 203 touching grains within 93 aggregates to plot the resulting contoured axis and angle distributions shown in Fig. 3. The same methodology was used to assess the misorientation signature of olivine dendrites (Fig. DR5).

In contrast, chromite neighbour pair misorientation measurements were calculated automatically from a single EBSD map of the entire thin section. Due to the presence of thousands of individual chromites in a single EBSD map, a higher threshold for the grain segmentation was used (8°), to automatically separate high and low angle grain boundaries.

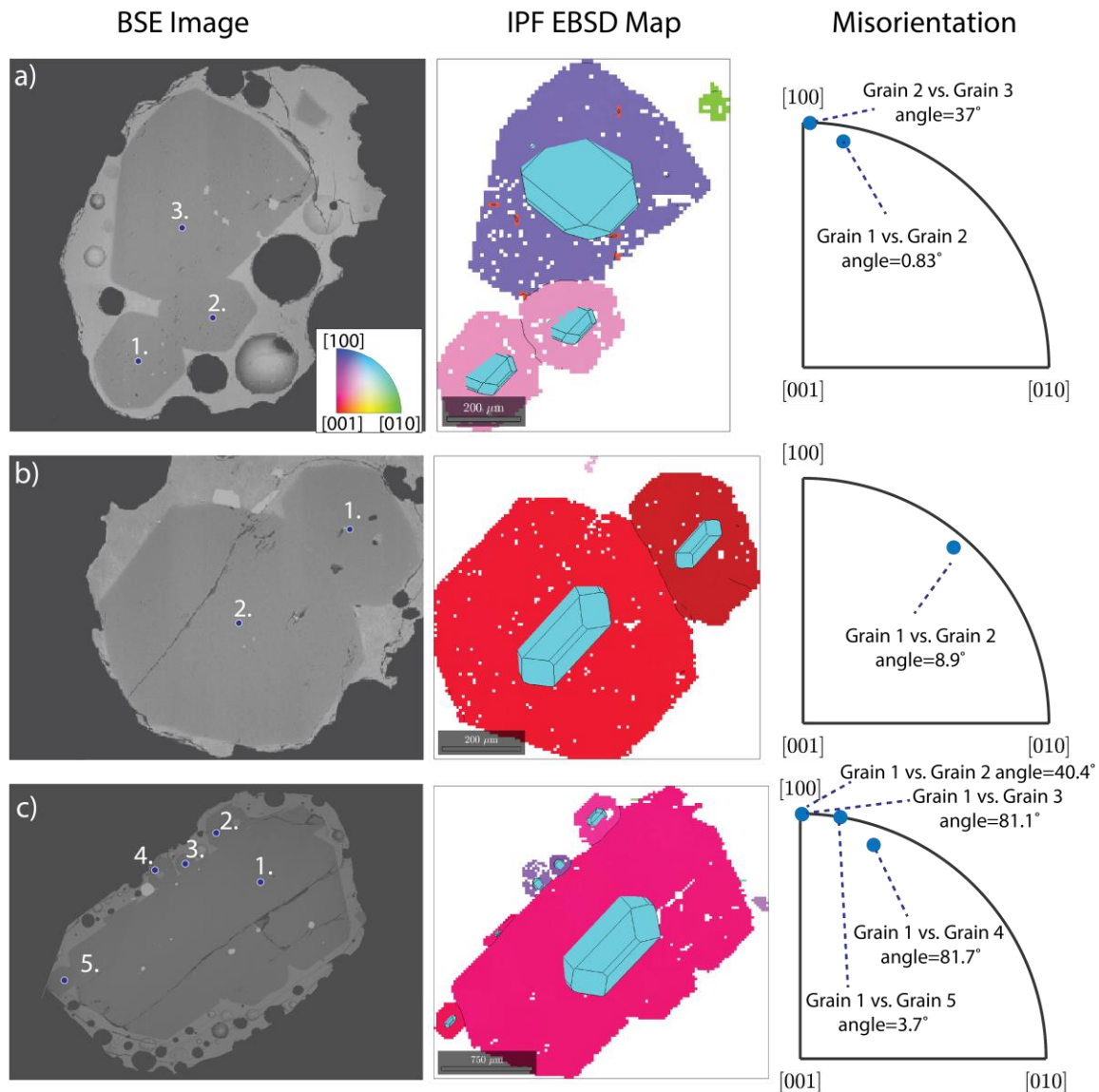


Fig. DR1 –Examples of the method used to quantify misorientations within individual olivine aggregates. BSE images (LHS) were used to identify boundaries between morphologically distinct crystals. EBSD maps (middle) are colored with respect to their orientation (e.g. red colors shows that the [001] axis is normal to the image plane). The orientation of each crystal can also be visualized from the 3D olivine shape superimposed in MTEX. Misorientations for each pair of touching grains are shown as axis-angle pairs (RHS). Individual measurements from 93 separate EBSD maps were combined to produce Fig. 3 in the main text. Note, the olivine geometry displayed using the crystalShape package expresses a large {120} face, and a smaller {110} face. Based on observations of aggregate morphology in Kilauean olivines, the {110} face is dominant, with a smaller {120} face (as shown in Fig. 3).

Normalising Misorientation Axes in Chromite aggregates

The density distribution of misorientation axes over the full angle range is not uniform for all crystallographic directions, even for uniformly distributed crystal orientations. This is due to the non-uniform misorientation angle distribution (i.e. the maximum misorientation angle). For example, for chromites, the maximum angle about $\langle 100 \rangle$ is 45° , about $\langle 111 \rangle$ is 60° , while the maximum possible misorientation angle of 62.8° in a cubic system can only be realised around $\sim \langle 773 \rangle$. Accordingly, misorientation axis close to $\langle 773 \rangle$ have a higher

probability of being encountered than other axes in a random sample of misorientations drawn from a uniform distribution. In contrast, axes with a smaller angular range (e.g. $\langle 100 \rangle$) will have a lower probability density. The non-uniform misorientation axis distribution is defined purely by the crystal symmetry, rather than the characteristics of the sample. Thus, the measured misorientation axis distribution should be normalized to this. Normalisation was performed by computing the spherical functions for each misorientation axis distribution, and dividing the measured distribution by this uniform-derived function, and normalising to a mean density of 1. This correction is particularly important in high symmetry minerals, such as chromite. For simplicity, olivine axes were left unnormalized, as the clustering of misorientation axes was so strong that normalizing to the uniform axis distribution was not significant.

Identifying Twin Laws

To identify potential twins in aggregates, a criterion was required to specify the permitted deviation from the ideal twin laws (Fig. DR2).

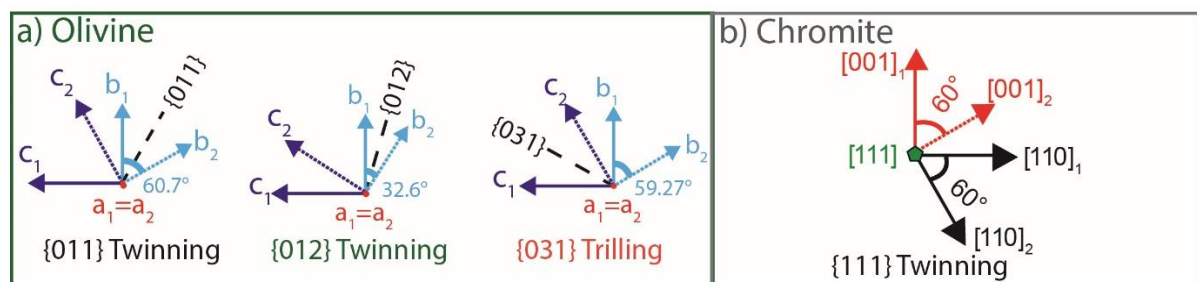


Fig. DR2 -Twin laws in olivine and chromite, after Dodd and Calef, 1971) and Deer (1966) respectively.

Crystals of cubic minerals such as chromites exhibit a special type of low energy boundary called coincidence site lattices (CSLs), where a finite number (Σ) of lattice points coincide along the boundary (Randle and Engler, 2000). The chromite twin law is the most common CSL with $\Sigma = 3$ (Garbacz and Grabski, 1989). The permitted deviation from these ideal CSLs (or twins) was calculated using Brandon's Law:

$$\vartheta = \vartheta_0 (\Sigma)^{-0.5}$$

where ϑ is the permitted deviation, ϑ_0 is the angle used to differentiate subgrain and true grain boundaries (8°), and Σ is the CSL number.

For the $\{111\}$ twin in chromites (CSL3), the permitted deviation is 4.61° . The application of Brandon's law (and thus CSL numbers) to systems with lower symmetry such as olivine is less well established. As an approximation, CSL numbers can be calculated based on the hexagonal cubic sublattice for planes of oxygen within olivine (Poirier, 1975). Using $\Sigma=3$ for $\{011\}$ twinning, and $\Sigma=39$ for $\{012\}$ twinning (Faul and Fitz Gerald, 1999), this permits angular deviations of 4.6° and 1.3° respectively from the ideal twin laws (when $\vartheta_0=8^\circ$).

Assessing Facial Attachments using crystalShape

The crystalShape MTEX class was used to superimpose 3D olivine crystals on 2D EBSD maps (https://mtextoolbox.github.io/files/doc/crystalShape_index.html). This, alongside BSE images showing the euhedral outlines of grains, allows assessment of facial attachments in approximately ~50% of aggregates (those with euhedral-subhedral crystal shapes). For examples, see Fig 1 in the text, and Fig. DR1 above.

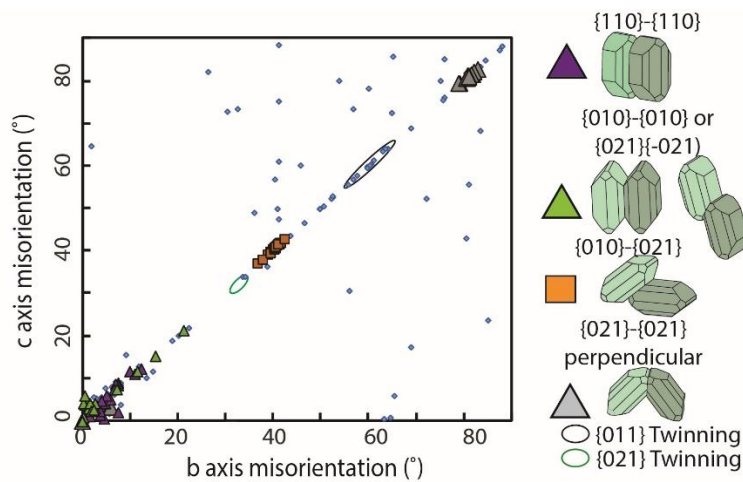


Fig. DR3 – There is an excellent correlation between the misorientation of the b and c axes of neighbouring crystals in olivine aggregates (resulting from the clustering of misorientation axes about $\langle 100 \rangle$). Grains where facial attachments could be assessed are indicated. Grains within the permitted deviation of olivine twin laws are circled.

CALCULATING SURFACE ENERGIES

SHAPE V7.4 (www.shapesoftware.com) was used to construct euhedral olivine and chromite crystals of known facial areas and volumes. For olivine, forsterite unit cell parameters were used ($a=4.756$, $b=10.195$, $c=5.981$ Å). The shape ratio was set at $a:b:c=1.5:1:2$, with the central distances ratios used by Welsch et al. (2013). For cubic chromite, only $\{111\}$ faces were expressed. Central distances were adjusted to produce a crystal with a volume of 1mm^3 (Fig. DR4).

The interfacial energy for a single crystal with a volume of 1mm^3 was calculated by multiplying the area of each face by the interfacial energy of that face. Central distances were then adjusted to yield a crystal with a volume of 0.5mm^3 . The total interfacial energy of two attached 0.5mm^3 crystals was calculated by multiplying the area of each face by its energy, minus the energies of the two attached faces.

For chromite, surface energies for NiFe_2O_4 spinel from Mishra and Thomas (1977) were used. However, as only $\{111\}$ faces are expressed, the ratio of aggregate:single crystal energies for chromite is not dependent on the choice of surface energy. For olivine, Ab initio surface energies of forsterite in a vacuum at 0 K were used (Bruno et al., 2014). As surface adsorption on olivine in basaltic melt is anisotropic (Wanamaker and Kohlstedt, 1991; de Leeuw et al., 2000), our calculated energy differences are reliant on the assumption that the relative magnitudes of facial energies are not affected by surface adsorption. However, as there are significant energy penalties for growth of a daughter crystal for all attachment faces, the conclusion that heterogeneous nucleation is energetically unfavourable is not sensitive to the exact choice of facial energies.

Table 1a – Calculations for single olivine crystal with a volume of 1mm^3 (morphology shown in Fig. DR4)

Face	Energy (J/m^2)	Number of faces	Total face area <i>Area of each face (mm^2) x # of faces</i>	Total energy per face (μJ) <i>Energy (J/m^2) x Area (mm^2)</i>
010	1.22	2	1.109	1.353
021	1.90	4	2.023	3.843
110	2.18	4	1.438	3.135
101	1.78	4	0.179	0.319
001	1.78	2	0.176	0.313
120	1.36	4	0.683	0.928
Total interfacial energy (sum of all 6 faces)				9.89 μJ

Table 1b– Calculation of the interfacial energy for an olivine aggregate consisting of two identical crystals (each with a volume of 0.5mm³) joined along the {010} face.

Face	Energy (J/m ²)	Number of faces	Total face area Area of each face (mm ²)x # of faces	Total energy per face (μJ) Energy (J/m ²)xArea (mm ²)
010	1.22	2	0.699	0.853
021	1.90	4	1.274	2.421
110	2.18	4	0.906	1.975
101	1.78	4	0.113	0.201
001	1.78	2	0.111	0.197
120	1.36	4	0.430	0.585
Total interfacial energy per crystal				6.23 μJ
Interfacial energy of two 010 faces				0.853 μJ
Total interfacial energy of aggregate <i>2 x Total energy per crystal – energy of 2 touching 010 faces</i>				11.6 μJ
aggregate energy/single crystal energy (%)				117%

Table 1c- Energy differences for aggregates joined along each of the 6 olivine crystal faces.

Attached Faces	{110}	{120}	{010}	{021}	{001}	{101}
aggregate energy/single crystal energy (%)	116%	123%	117%	114%	124%	125%

Table 1d– Calculations for single chromite crystal with a volume of 1mm³ (morphology shown in Fig. DR4)

Face	Energy (J/m ²)	Number of faces	Total face area Area of each face (mm ²)x # of faces	Total energy per face (μJ) Energy (J/m ²)xArea (mm ²)
{111}	0.207	8	5.719	1.184
Total interfacial energy				1.18 μJ

Table 1e– Calculation of the interfacial energy for a chromite aggregate consisting of two identical crystals (each with a volume of 0.5mm³) joined along the {111} face.

Face	Energy (J/m ²)	Number of faces	Total face area Area of each face (mm ²)x # of faces	Total energy per face (μJ) Energy (J/m ²)xArea (mm ²)
{111}	0.207	8	3.603	0.746
Total interfacial energy per crystal				0.746 μJ
Interfacial energy of two 111 faces				0.186 μJ
Total interfacial energy of aggregate <i>2 x Total energy per crystal – energy of 2 touching 111 faces</i>				1.31 μJ

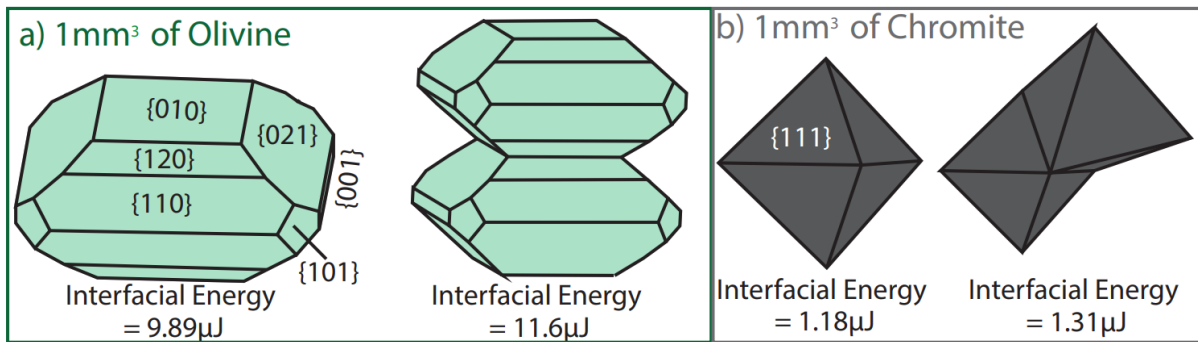


Fig DR4– Crystal geometries used for interfacial energy calculations (produced in SHAPE V7.4).

MISORIENTATION SIGNATURES OF OLIVINE DENDRITES

Misorientations in branching olivine dendrites from West Greenland Picrites (Larsen and Pederson, 2000) were quantified to assess whether olivine aggregates represent texturally matured dendrites (as suggested by Welsch et al., 2013).

N=125

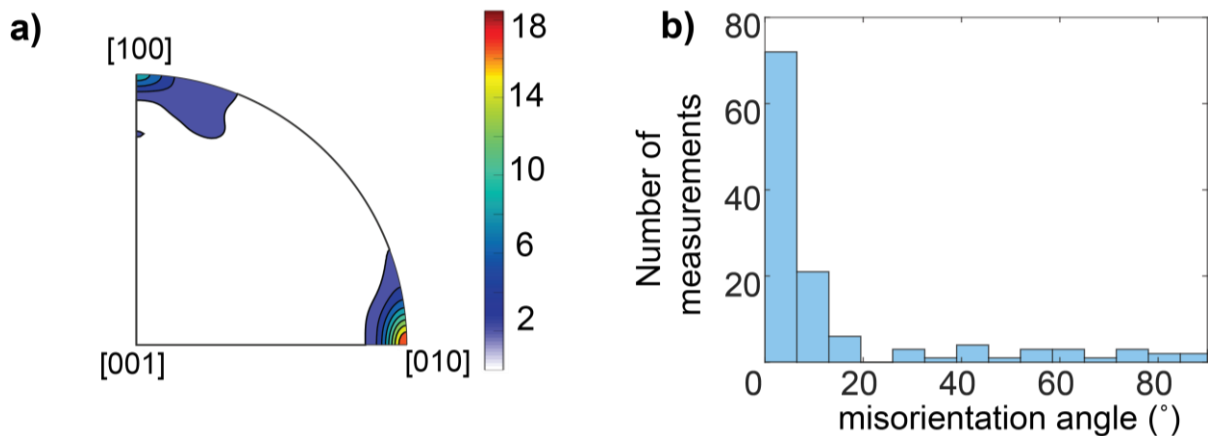


Fig DR5– a) Misorientation axes for 125 dendritic buds displaying non crystallographic branching cluster strongly at [010] (as reported by Donaldson, 1976), with a weak secondary maxima at [100] (previously unreported). The color scale in a) has units of ‘multiples of uniform distribution’. b) Misorientation angles show a peak at $<10^\circ$, but a relatively uniform distribution at higher angles. This is in clear contrast to the multiple misorientation peaks observed in Kīlauean aggregates.

ADDITIONAL REFERENCES

Bruno, M., Massaro, F.R., Prencipe, M., Demichelis, R., De La Pierre, M. and Nestola, F., 2014. Ab Initio calculations of the main crystal surfaces of forsterite (Mg_2SiO_4): a preliminary study to understand the nature of geochemical processes at the olivine interface. *The Journal of Physical Chemistry C*, 118(5), pp.2498-2506.

De Leeuw, N.H., Parker, S.C., Catlow, C.R.A. and Price, G.D., 2000. Modelling the effect of water on the surface structure and stability of forsterite. *Physics and Chemistry of Minerals*, 27(5), pp.332-341.

Faul, U.H. and Gerald, J.D.F., 1999. Grain misorientations in partially molten olivine aggregates: an electron backscatter diffraction study. *Physics and Chemistry of Minerals*, 26(3), pp.187-197.

Garbacz, A., and M. W. Grabski. 1989. Modelling of CSL boundaries distribution in polycrystals. *Scripta metallurgica* 23(8), pp. 1369-1374.

Poirier, J.P., 1975. On the slip systems of olivine. *Journal of Geophysical Research*, 80(29), pp.4059-4061.

Mishra, R.K. and Thomas, G., 1977. Surface energy of spinel. *Journal of Applied Physics*, 48(11), pp.4576-4580.

QUANTAX CrystAlign. Bruker Nano GmbH, Berlin, Germany, 2010.

Randle, V. and Engler, O., 2000. *Introduction to Texture Analysis: Macrotecture, Microtexture and Orientation Mapping*. Gordon & Breach Science Publishers. Reading, UK.

Veksler, I.V., Sedunova, A.P., Darin, A.V., Anosova, M.O., Reid, D.L., Kaufmann, F.E., Hecht, L. and Trumbull, R.B., 2018. Chemical and textural re-equilibration in the UG2 chromitite layer of the Bushveld Complex, South Africa. *Journal of Petrology*.

Wanamaker, B.J. and Kohlstedt, D.L., 1991. The effect of melt composition on the wetting angle between silicate melts and olivine. *Physics and Chemistry of Minerals*, 18(1), pp.26-36. <https://doi.org/10.1007/BF00199040>